SOMI
CONGRESO DE INSTRUMENTACIÓN
Año 4, No. 01, octubre 2017
ISSN 2395-8499

Low-cost CMOS active pixel Sun Sensor for nanosatellite's two-axis attitude determination.

Jorge Prado-Molina, Héctor Arriaga-Arrollo and Julio-César Balanzá-Ramagnoli.
jprado@igg.unam.mx bolsonsurvive@hotmail.com jc.balanza.r@gmail.com
Instituto de Geografía, Universidad Nacional Autónoma de México,
Mexico City, Mexico.

ABSTRACT

This paper describes the design, construction, and Laboratory testing of a high precision CMOS active pixel Sun sensor. This device was developed at the Institute of Geography of the National Autonomous University of Mexico (UNAM). The two-axis CMOS active pixel Sun sensor developed has a precision of ± 0.05° and employs a bidimensional array of 5 Mpixels with a field of view (FOV) of ± 50.83° and ± 78.48°. A pinhole with a small aperture of 400µm, is placed at a distance of 3 mm from the CMOS detector. The centroid method was used to determine the illuminated pixel of the bidimensional sensing array. Other options like thresholding, filtering, and template method, were considered. These last methods are quite susceptible to noise detecting the sunlight intensity. CMOS active pixel Sun sensors are basic components to determine on-orbit attitude of nanosatellites using the Sun as a positional reference. This sensor represents a common and reliable technology, employed in many space missions and applications owing to their simple manufacturability, limited size, and low weight.
Results obtained in attitude determination were compared against a high precision, high accuracy electronic compass.
KEYWORDS: CubeSat, microsatellites, Sun Sensor, CMOS active pixel.

1 INTRODUCTION

For satellite attitude determination, there are different sorts of sensors, such as: magnetometers, star trackers, gyroscopes, horizontal scanners, Earth and Sun sensors, all depending on measured rates or reference vectors [1]. Active pixel Sun sensor determines the satellite´s attitude by measuring the Sun vector. This sensor employs simple designs, it is of low-cost and widely used on nanosatellites, due to their simple manufacturability, limited size, low-weight and low power consumption [2]. CMOS active pixel bidimensional Sun sensor detects and calculates the sunlight incident angle using the projected sunlight image on this device. The basic characteristics of the CMOS active pixel Sun sensor are showed on Table 1. Therefore,

ISSN 2395-8499

accuracy is the most important factor in Sun sensor development. The two axis CMOS Sun sensor designed and developed and described in this paper has good resolution and is adequate for many space missions and applications.

Table 1. Main characteristics of the CMOS active pixel Sun sensor

Focal length	3 mm
Field of view (FOV)	± 50.83° * ± 78.48°
Mask	
Material	brass
Thickness	400µm
Numbers of pinholes	1
pinhole diameter	400µm
Photodetector	
Technology	CMOS active pixel sensor
Brand	ON Semiconductor
Model	MT9P031I12S
Resolution	2592 H *1944 V pixels (5 Mpixels)
Pixel size	2 * 2 µm
Sensing area size	5.70 mm * 4.28 mm
ADC resolution	12 bits
Responsivity	1.4 V/lux-sec (550 nm)
Pixel dynamic range	70.1 dB
SNR maximum	38.1 dB
Operating temperature	-30 °C to +70°C
Power consumption	381 mW at 14 fps full resolution

2 METHODS TO CALCULATE THE CENTROID

In order to calculate the incident angle of the sunlight using the sunlight image, the centroid of the image onto the CMOS image sensor must be found. There are many algorithms employed

SOMI
CONGRESO DE INSTRUMENTACIÓN
Año 4, No. 01, octubre 2017
ISSN 2395-8499

to obtain the centroid [3-8] and some different methods to determine the illuminated pixels in the electronic image array. Those will be mentioned at the end of this section.

2.1 Method employed to calculate the centroid

The basic method to calculate the centroid is shown in figure 1. The centroid (*Xp,Yp*) of the projected image onto the CMOS image sensor can be found using equations 1 and 2:

$$x_p = \frac{\left(\sum_{i=1}^{N} x_i I_i\right)}{\left(\sum_{i=1}^{N} I_i\right)} \tag{1}$$

$$y_p = \frac{\left(\sum_{i=1}^{N} y_i I_i\right)}{\left(\sum_{i=1}^{N} I_i\right)} \tag{2}$$

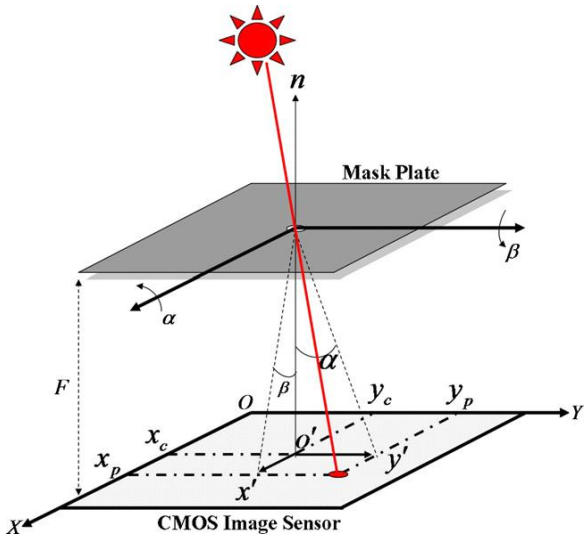

Figure 1. Basic principle of operation of the Sun sensor. Sun's rays passes over the pinhole and are detected by the CMOS bidimensional array. This device is scanned and the illuminated pixel's positions calculated and then the two-axis attitude established.

Relationship between the centroid of the image of the Sun and the incident angle of the Sun's rays are described by the next equations:

$$x' = -F \tan\beta \tag{3}$$

ISSN 2395-8499

$$y' = -F \tan \alpha \quad (4)$$

$$x' = x_p - x_c \quad (5)$$

$$y' = y_p - y_c \quad (6)$$

$$\alpha = \tan^{-1}\left(\frac{x_p - x_c}{F}\right) \quad (7)$$

$$\beta = \tan^{-1}\left(\frac{y_p - y_c}{F}\right) \quad (8)$$

where:

(x_i, y_i) denotes the location of each pixel,

(x_c, y_c) is the centre of the CMOS active pixel sensor,

(x_p, y_p) is the centroid of the image projected by the sun's rays,

I_i is the intensity of the image of the Sun,

α incident angle on the x-axis [°],

β angle incident on the y-axis [°],

F distance between the aperture of the mask and the CMOS sensor (focal length) [mm],

$O - X - Y$ axis of CMOS active pixel sensor.

x', y' are the differences between the centre of the sensor and the centroid of the projected image [mm].

This method can effectively compensate for the noise in the data and also it can calculate the centroid with high accuracy. Other methods were reviewed, however, the above mentioned was chosen, because of the advantages offered.

2.2 Other methods to establish the centroid

2.2.1. Threshold method employed to calculate the centroid of the image

The threshold method is the most simple and easy to implement. Accuracy changes according to the threshold level. This method is expressed using equations 9, 10, and 11:

ISSN 2395-8499

$$x_p = \frac{\left(\sum_{i=1}^{N} x_i I_i'\right)}{\left(\sum_{i=1}^{N} I_i'\right)} \quad (9)$$

$$y_p = \frac{\left(\sum_{i=1}^{N} y_i I_i'\right)}{\left(\sum_{i=1}^{N} I_i'\right)} \quad (10)$$

$$I_i' = I_i - \mu I_{\max}; I' \succ 0 \quad (11)$$

where:

μ determines the threshold value, all data below it are converted into a digital logic zero. If the image of the sunrays contains noise, an appropriate value must be selected to remove it. However, it is difficult to determine an optimal threshold value.

2.2.2. Filtering method to calculate the centroid

The filtering method utilizes image processing that removes noise by using smoothing filters in a pre-process phase before applying the basic method. The original intensity data of the pixel or pixels of interest, takes a new value considering the pixel's adjacent average intensity. This method is described with equation 12:

$$I_{m,n} = \frac{1}{9} \sum_{i=m-1}^{m+1} \sum_{j=n-1}^{n+1} I_{i,j} \qquad (1 \le m \le 256 \qquad 1 \le n \le 256) \quad (12)$$

where:

$I_{m,n}$ is 0, if "i" and "j" are less that 1,

"i" and "j" are the location of the pixels in "X" and "Y".

Threshold and filtering and methods are quite susceptible to noise detecting sunlight intensity.

3 PHYSICAL DESIGN OF THE SUN SENSOR

In this section mechanical design of the sun sensor is described.

SOMI
CONGRESO DE INSTRUMENTACIÓN
Año 4, No. 01, octubre 2017
ISSN 2395-8499

3.1 Errors to be taken into account for physical design

Figure 2 shows the design of the mask of the sun sensor. It consists of a plate having a pinhole of 400µm diameter and thickness, with a distance from the mask to the CMOS detector of 3 mm.

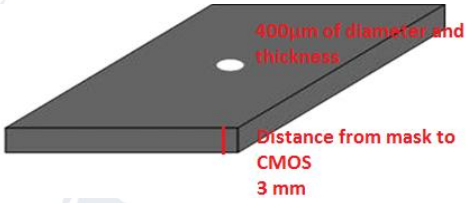

Figure 2. Physical design of the mask, thickness is the same as the diameter of the pinhole.

There are some errors that must be considered in the Sun sensor model, such as: geometric errors caused by misalignment during fabrication and mask placement, and errors caused by electronic noise in the circuits [2]. Optical errors are caused by imperfection in the aperture geometry (shadow effects). Blocking the aperture at a high incidence angle affects the accuracy of the Sun sensor, this is known as the shading effect and to avoid this, it is very important to reduce its thickness. This can be observed in equations 13 and 14 and in figure 3.

$$w = \ell + \delta \tag{13}$$

$$\delta = d \left| \tan\theta \right| \tag{14}$$

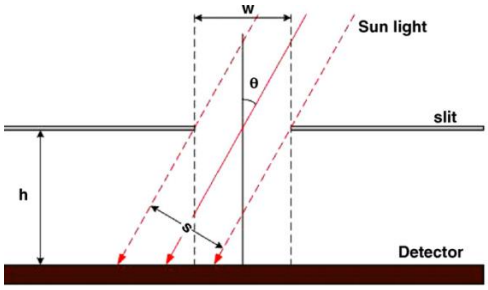

Figure 3. Errors to be taken into account for physical design. Shading effect is one of the most important.

To calculate the angular size from a source at an infinite distance, we use equation 15:

$$\theta_s = 2\tan^{-1}\left(\frac{R}{F}\right) \tag{15}$$

where:

SOMI
CONGRESO DE INSTRUMENTACIÓN
Año 4, No. 01, octubre 2017
ISSN 2395-8499

θ_s is the angular size of a source at an infinite distance [°]
θ is the projection angle of the Sun [°],
R is the radius of the angular aperture [mm],
F is the focal length [mm],
w is the diameter of the circular aperture [mm],
δ is the shading effect [mm],
d is the width of the mask [mm],
l is the width, without the effects of shading [mm].

4 EXPERIMENTAL SETUP

4.1 PCB design and construction.

In the market there are two basic types of bidimensional imaging sensors available: CCDs and CMOS. Nowadays, the CMOS is a cheaper and reliable technology, employed in many space missions and applications thanks to their advantages over CCD devices. Specifications of the chosen commercial CMOS active pixel sensor are shown on table 1. The PIC18F4550 microcontroller is employed to generate clock signals at 3 MHz and PIC32MZ2048EFH100 houses the algorithm to calculate the two-axis orientation using the Sun's rays passing through the pinhole in the upper part of the sensor. PCB card is 45.67 mm long and 47.95 mm wide. Figure 4 shows both sides of the PCB, on the left side the CMOS bidimensional sensor is located. On the right side two microcontrollers execute the scanning process to read the illuminated pixels of the CMOS active pixel sensor, and the other the algorithm to determine the position of the sunrays striking the sensor and then the two-axis orientation.

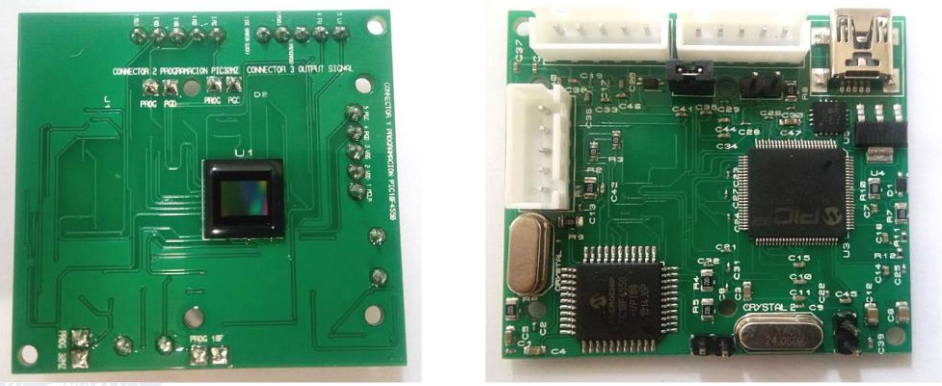

Figure 4. Both sides of the PCB housing all the electronic components of the Sun sensor.

SOMI
CONGRESO DE INSTRUMENTACIÓN
Año 4, No. 01, octubre 2017
ISSN 2395-8499

4.2 CMOS active pixel Sun sensor alignment mask.

Figure 5 shows the alignment system located in the upper part of the CMOS active pixel Sun sensor. This device is employed to effectively align the mask with the center of the CMOS detector to eliminate errors caused by misalignment.

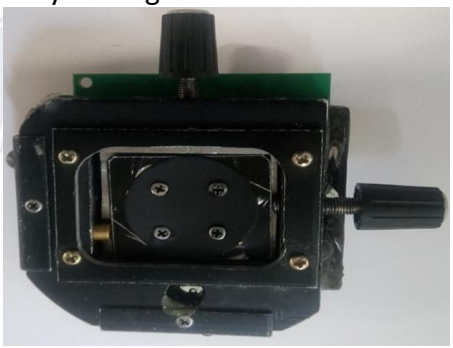

Figure 5. CMOS active pixel Sun sensor's mask positioning device.

5 RESULTS

Functioning tests were performed in the Laboratory, orientation angles were measured with an electronic compass (AOSI, model EZ-compass 4) it has a resolution of 0.08° [9-10]. The results showed on graphs are the averages and their corresponding standard deviation of α and β angles of 15 measurements taken. The results of α angle are shown on the figure 6, meanwhile results obtained measuring β angle are depicted on figure 7.

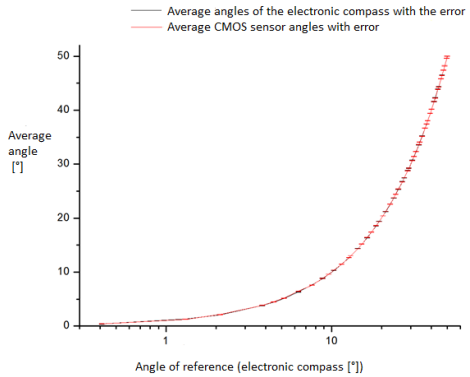

Figure 6. Results obtained with the Sun sensor, measuring α angle, and comparing them with the lectures of the electronic compass used as reference.

ISSN 2395-8499

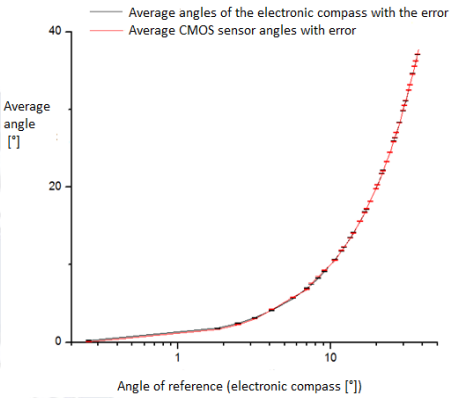

Figure 7. Results obtained with the Sun sensor, measuring β angle, and comparing them with the lectures of the electronic compass used as reference. Graph also depicts standard deviation.

6 CONCLUSIONS

In this paper we analyzed and compared four different methods to determine the two-axis attitude for a nanosatellite using the Sun as a reference and a bidimensional electronic imaging sensor. A new algorithm was developed that drastically reduce the computational load to the on-board computer. The maximum error exhibited by the CMOS sensor was in the angles near the origin, so decreasing the diameter of the pinhole and the thickness of the mask, would increase the accuracy and therefore, reduce the error, considerably. The primary objective of the project was accomplished reaching the goals to design, construct, and test the operation of a Sun sensor with an accuracy of less than or equal to ± 0.05° and a maximum absolute error of 0.168° in both angles: α and β. This device is capable to support the attitude stabilization required by a remote sensing equipment mounted in a nano-satellite.

7 ACKNOWLEDGEMENT

To CONACYT (National Council for Science and Technology, Mexico) for their support throughout the project: “Prototipo Funcional de un Sistema de Estabilización Satelital Triaxial” AEM-2014-01-247812.

8 REFERENCES

[1] Prado, Jorge. (2007). Simulation system for testing algorithms for orientation and control of small satellites (PHD thesis). UNAM. Mexico City.

ISSN 2395-8499

[2] Arriaga Arroyo, Héctor Hugo. (2013) Solar sensor based on a two-dimensional active pixel arrangement to obtain two-axed attitude on a satellite (master thesis). UNAM. Mexico City University City.
[3] K. D. Mielenz. (1998). Algorithms for Fresnel diffraction at rectangular and circular apetures, Journal of reseach of the national institute of standards and technology vol. 103.
[4] Young-Keun, Chang; Byung,-Hoon, Lee. (2006). A new modeling and validation of two-axis miniature fine sun sensor. Elsevier, School of Aerospace and Mechanical Engineering, Korea Aerospace University, Hwajeon-dong, Duckyang-gu,Goyang-City 412-791, Republic of Korea, pp 357-365.
[5] Christian Liebe, Carl; Mobasser, Sohrab. (2001). MEMS Based Sun Sensor, Jet Propulsion Laboratory, California Institute of Technology, 4800 Oak Grove Dr, Pasadena CA 91 109-8099, USA, Part 3, p. 1565-1572.
[6] Young-Keun, Chang; Byung,-Hoon, Lee. (2007). Development of high-accuracy image centroiding algorithm for CMOS-based digital sun sensors, Elsevier, School of Aerospace and Mechanical Engineering, Korea Aerospace University, Hwajeon-dong, Duckyang-gu,Goyang-City 412-791, Republic of Korea, pp 29-37.
[7] Xie, Ning; Albert J.P., Theuwissen. (2011). An Autonomous low power high resolution micro- digital sun sensor, Proc. Of SPIE Vol. 8194, pp. 81941F1 to 81941F8, Belgium.
[8] Rufino, Giancarlo; Grassi, Michele. (2004). Development and Validation of a Modern CMOS Digital Sun Sensor at UniNa, Department of Aerospace Engineering, University of Naples Federico II, Naples, Italy.
[9] Advanced Orientation Systems, Inc. (2014). EZ-Compass-4 Miniature Tilt Compensated Compass [online]. [Review date: 11 September 2016]. Available at: http://www.aositilt.com/compass/ez-compass-4/.
[10] Advanced Orientation Systems, Inc. (2015). EZ-Compass-4 Miniature Tilt Compensated Compass [online, PDF file]. [Review date: 11 September 2016]. Available at: http://198.171.212.28/files/1814/4621/7614/APPCOMP4_USER_new_AOSI_manual.pdf.